

## Low Band Gap Poly(thienylene vinylene)/Fullerene Bulk Heterojunction Photovoltaic Cells

Jung Yong Kim,<sup>†</sup> Yang Qin,<sup>‡</sup> Derek M. Stevens,<sup>†</sup> Ozan Ugurlu,<sup>§</sup> Vivek Kalihari,<sup>†</sup> Marc A. Hillmyer,<sup>‡</sup> and C. Daniel Frisbie\*,<sup>†</sup>

Department of Chemical Engineering and Materials Science, University of Minnesota, 421 Washington Avenue SE, Minneapolis, Minnesota 55455, Department of Chemistry, University of Minnesota, 207 Pleasant Street SE, Minneapolis, Minnesota 55455, and Characterization Facility, Shepherd Laboratories, University of Minnesota, 100 Union Street SE, Minneapolis, Minnesota 55455

Received: March 11, 2009

Semicrystalline poly(3-hexyl-2,5-thienylene vinylene) (P3HTV) with a low band gap of 1.65 eV has been synthesized by acyclic diene metathesis polymerization and incorporated into bulk heterojunction (BHJ) organic solar cells. The polymer was thermally characterized by differential scanning calorimetry and thermogravimetric analysis and was blended with the electron acceptor methanofullerene [6,6]-phenyl C<sub>61</sub>-butyric acid methyl ester (PCBM) to make a light-harvesting charge-transfer thin film. The properties of P3HTV/PCBM blends were studied as a function of PCBM composition by wide-angle X-ray scattering, atomic force microscopy, transmission electron microscopy, UV-vis absorption spectroscopy, and charge-transport and photovoltaic measurements. The PCBM solubility limit, that is, the phase separation point, was estimated to be 50 wt % PCBM. The phase behavior of the blend was directly correlated with electrical transport behavior in a field-effect transistor testbed. At the phase separation point, charge carrier transport switches from hole only to ambipolar (both electron and hole) due to the formation of an electron-transporting percolating network of PCBM domains. BHJ solar cells were constructed with P3HTV films blended with varying weight fractions of PCBM. In these cells, spun-cast films of P3HTV/PCBM mixtures were sandwiched between poly(3,4-ethylene dioxythiophene)/poly(styrenesulfonate) (PEDOT/PSS)-coated ITO and Al electrodes. The best performance of polymer solar cells was observed at 50–60% PCBM, near the phase separation point at which power conversion efficiencies of 0.80–0.92% were measured under AM 1.5, 100 mW/cm<sup>2</sup> illumination.

### Introduction

Conjugated polymer/fullerene bulk heterojunction (BHJ) solar cells have received increased attention because of their promising energy conversion efficiencies, solution processability, and the potential for low cost fabrication.<sup>1–14</sup> Power conversion efficiencies (PCEs) of more than 5% have been reported in state-of-the-art BHJ cells incorporating the widely used electron donor polymer poly(3-hexylthiophene) (P3HT).<sup>5–14</sup> However, to achieve PCE values higher than 10%, optimization of nanoscale morphology, transport properties, band gap, band alignment, and device architecture must occur.<sup>4,15,16</sup>

The PCE is directly proportional to the short circuit current ( $J_{sc}$ ), open circuit voltage ( $V_{oc}$ ), and fill factor (FF) of the device. A key strategy to increase  $J_{sc}$  is to use low band gap ( $E_g$ ) polymers to harvest a greater fraction of the incident solar photon flux than is currently captured.<sup>17–24</sup> As a simple example, if we assume 100% quantum efficiencies for all energies above the band gap (similar to the case of inorganic semiconductors), reducing  $E_g$  from 1.91 eV (P3HT) to just 1.65 eV, in principle, can increase the integrated  $J_{sc}$  from the standard AM 1.5 Global solar spectrum (100 mW/cm<sup>2</sup>) from 17 to 24 mA/cm<sup>2</sup>.<sup>25</sup> Importantly, the effect of reducing the band gap on the ionization potential must be taken into consideration, as  $V_{oc}$  varies linearly with the difference between the donor HOMO level and acceptor LUMO.<sup>16</sup> In addition, to obtain high  $J_{sc}$  and FF, solar cells must

be efficient at separating excitons and avoiding carrier recombination.<sup>10,20</sup> Provided the donor/acceptor morphologies can be optimized, semicrystalline polymers are, in general, more attractive for this purpose than amorphous materials due to their enhanced charge-transport properties.

Several low band gap conjugated polymers ( $E_g < 1.8$  eV) have been employed as electron donor materials in BHJ solar cells.<sup>17–24,26–35</sup> Among these, benzothiadiazole-based copolymers were the most successful showing a PCE in the range of ~1.0–5.5%.<sup>21,23,28–29</sup> The reasons for such high performance might be ascribed to the material properties, such as high hole mobilities ( $\mu_h = 2 \times 10^{-2}$  cm<sup>2</sup>/(V s)), structural stability in the charged state, as well as a broad absorption spectrum ( $E_g \sim 1.38$  eV).<sup>21</sup> In this work, we have used another potentially important material, poly(thienylene vinylene) (PTV), with  $E_g \sim 1.65$  eV for BHJ solar cells. PTV is a known low  $E_g$  polymer with good transport properties ( $\mu_h = 1.5 \times 10^{-3}$  cm<sup>2</sup>/(V s)).<sup>30–38</sup> Thus, PTV has the possibility, if well-optimized, to combine the strong points of P3HT demonstrated in polymer solar cells (e.g., good mobility and favorable morphology) while also decreasing the band gap.

Up to now, most PTV-based solar cells have incorporated polymers synthesized from precursor routes, which offer limited molecular weight control and have processing drawbacks originating from an additional heating process required to form extended  $\pi$  conjugation by elimination of a volatile leaving group.<sup>36–38</sup> In the devices reported here, we have employed a soluble PTV derivative, poly(3-hexyl-2,5-thienylene vinylene) (P3HTV), synthesized by a different method, acyclic diene metathesis (ADMET) polymerization.<sup>39,40</sup> ADMET methods

\* Corresponding author. E-mail: frisbie@chem.umn.edu.

<sup>†</sup> Department of Chemical Engineering and Materials Science.

<sup>‡</sup> Department of Chemistry.

<sup>§</sup> Shepherd Laboratories.

require low levels of catalyst, generally proceed under mild conditions, and allow for improved control over polymer molecular weight. We have made thin film blends of P3HTV and the electron acceptor methanofullerene [6,6]-phenyl C<sub>61</sub>-butyric acid methyl ester (PCBM), focusing on a thorough examination to characterize phase behavior across the composition range (Figure 1). Blend morphologies and crystal structures have been characterized using AFM, TEM, and WAXS to identify the solubility limit required for phase separation. The dependence of hole and electron transport on this phase separation was examined through field effect transistor measurements. Finally, we comprehensively investigated the BHJ solar cell performance of these blends as a function of increasing PCBM composition,<sup>41,42</sup> light intensity,<sup>43–49</sup> and photoactive layer thickness.<sup>50–52</sup> Importantly, both ambipolar charge transport and optimum solar cell performance were observed at the point of phase separation, illustrating the crucial role of this parameter in device design.

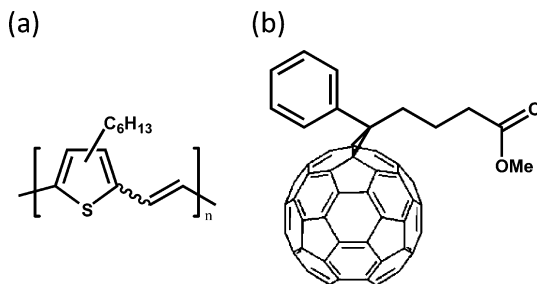


**Figure 1.** Chemical structures of (a) P3HTV and (b) PCBM.

## Experimental Section

**Materials.** P3HTV ( $M_n = 4.5$  kg/mol,  $M_w = 5.4$  kg/mol, polydispersity index (PDI) = 1.2 by size exclusion chromatography versus polystyrene standards, HOMO = -5.0 eV, LUMO = -3.3 eV) used in the current study was synthesized by ADMET polymerization of 2,5-dipropenyl-3-hexylthiophene, which will be described elsewhere.<sup>39,40</sup> PCBM was purchased from American Dye Source. PEDOT/PSS (Baytron P VP Al 4083) was purchased from H. C. Starck. ITO glass slides (sheet resistance, 8–12 Ω/cm<sup>2</sup>) were obtained from Delta Technologies. Heavily doped p-type Si wafers were obtained from Silicon Valley Microelectronics.

**Transistor Fabrication.** The SiO<sub>2</sub> side of the heavily doped p-type Si substrate was exposed to saturated hexamethyldisilazane (HMDS) vapor for several minutes.<sup>53,54</sup> On top of this surface, a few drops of 0.5 wt % polymer/fullerene solution (P3HTV/PCBM in *o*-dichlorobenzene (DCB)) were deposited and spin-coated at 2000 rpm for 60 s in ambient laboratory conditions. The spun polymer/fullerene films were ca. 20 nm thick. The blend films were annealed at 150 °C for 24 h. Gold top contact, source, and drain electrodes were formed by vacuum evaporation of 45 nm Au through a Si stencil mask. The finished transistor had a channel width of 4000 μm and a length of 40 μm.

**Photovoltaic Device Fabrication.** Photovoltaic (PV) devices were fabricated on pre-cleaned patterned ITO glass substrates. PEDOT/PSS was spin-coated on the ITO glass slides (2.54 × 2.54 cm<sup>2</sup>) at a speed of 4000 rpm for 45 s and annealed at ~120 °C for 5 min.<sup>53</sup> The PEDOT/PSS film was ~30 nm thick. On top of the PEDOT/PSS, a few drops of P3HTV/PCBM (concn ~ 1.0–5.5 wt %) in DCB were deposited and then spin-coated at a speed of 600 rpm for 60 s inside a glovebox. The spun

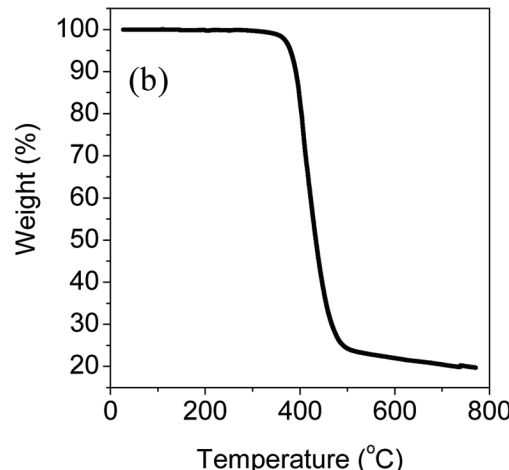
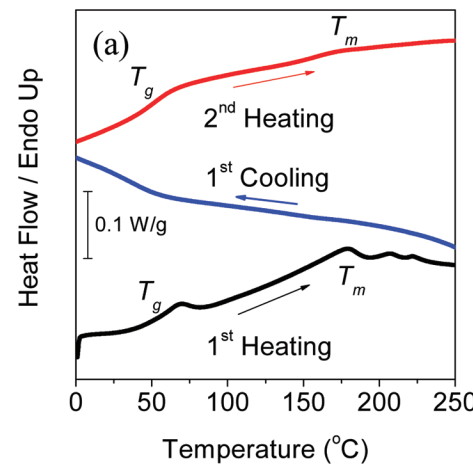


**Figure 2.** Thermal behavior of P3HTV at a scan rate of 10 °C/min: (a) DSC thermogram under N<sub>2</sub>, (b) TGA thermogram under N<sub>2</sub>.

P3HTV/PCBM films were ~200 nm ( $\pm 10$  nm) thick (for composition dependence of solar cell performance) or ~70–320 nm thick (for thickness dependence), which were measured using a KLA Tencor P-10 profilometer. After drying overnight by slow solvent evaporation, the spun film was mounted inside the bell jar of a Denton Vacuum Bench Top Turbo III thermal evaporator. Aluminum was evaporated to deposit a 100 nm thick electrode on top of the P3HTV/PCBM films. The device active area was 9 mm<sup>2</sup>.

**Characterization.** Thermal behavior was measured using differential scanning calorimetry (DSC, TA Instruments), and thermogravimetric analysis (TGA, PerkinElmer TGA 7). Melting temperatures were taken as peak maxima, and glass transition temperatures were taken as the midpoint between the two tangential baselines using the Universal Analysis 2000 software. Wide-angle X-ray scattering (WAXS) (Bruker-AXS microdiffractometer with 2.2 kW sealed Cu Kα X-ray source) was performed to check the molecular packing state of drop-cast P3HTV/PCBM films with a thickness of ca. 4 μm. Atomic force microscopy (AFM) images were taken with a Veeco Metrology Nanoscope IIIa microscope operating in tapping mode. Transmission electron microscopy (TEM) was accomplished with a FEI Tecnai T12 TEM at 80 kV under bright field. For TEM samples, the PV devices (without an Al top contact) were immersed into deionized water, and the spin-coated P3HTV/PCBM films were floated onto the water and collected by a 300 mesh copper grid.

Electrical characterization of transistors was performed in the dark using a Desert Cryogenics probe station with a base

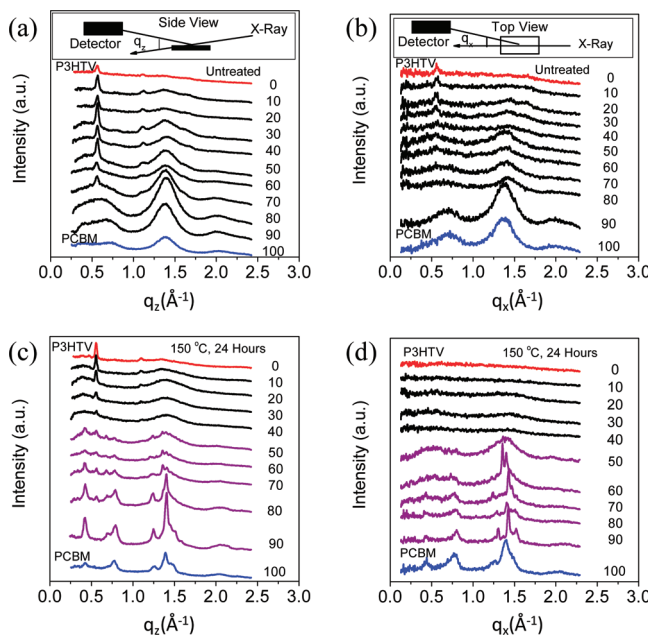


**Figure 3.** Room-temperature WAXS pattern for the drop-cast P3HTV/PCBM film as a function of PCBM wt %: (a) out-of-plane WAXS pattern for the untreated films, (b) GIXS pattern for the untreated films, (c) out-of-plane WAXS pattern for the annealed films ( $150\text{ }^\circ\text{C}$ , 24 h), and (d) GIXS pattern for the annealed films ( $150\text{ }^\circ\text{C}$ , 24 h).

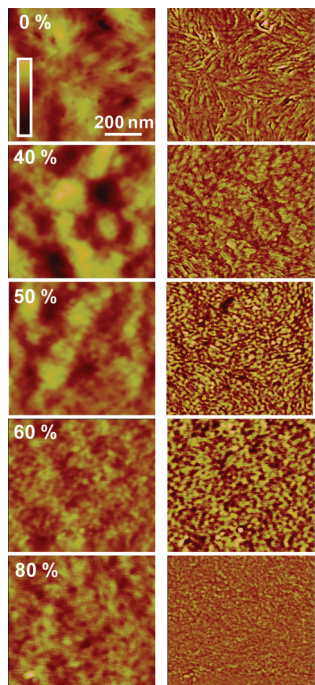


**Figure 4.** AFM tapping mode height (left column) and simultaneously acquired phase images (right column) of the P3HTV/PCBM blend films of various compositions. All the images are  $1 \times 1 \mu\text{m}^2$ , and the various compositions shown in the figures correspond to PCBM wt % in the P3HTV/PCBM blend. Image height range (maximum peak to valley) is 40 nm (0%), 25 nm (40%), 12 nm (50%), 7 nm (60%), and 5 nm (80%).

pressure of  $5 \times 10^{-7}$  Torr. Mobility ( $\mu$ ) was calculated in the linear regime using the equation  $\mu = |dI_D/dV_G|_{V_D=\text{const}}/(C_i V_D W/L)$ , where  $I_D$ ,  $V_G$ ,  $V_D$ , and  $C_i$  are drain current, gate voltage, drain voltage, and gate insulator  $\text{SiO}_2$  capacitance, respectively. For PV measurements, the illumination source was a 150 W Xe arc lamp (Oriel) with an AM 1.5G filter. Several attenuators with constant optical density were used to obtain the range of

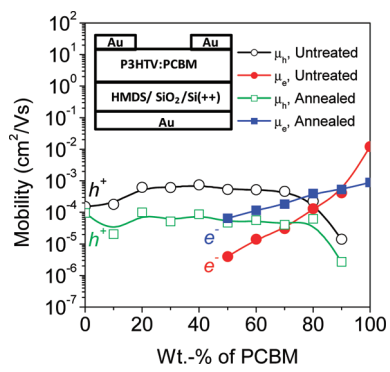


**Figure 5.** Linear mobility ( $\mu_h$  at  $V_D = -15\text{ V}$ ,  $\mu_e$  at  $V_D = 15\text{ V}$ ) of the P3HTV/PCBM blends as a function of increasing PCBM wt %. Annealing process was done at  $150\text{ }^\circ\text{C}$  for 24 h. Inset: P3HTV/PCBM transistor with a gold bottom gate.

light intensities. Current–voltage characteristics of PV cells were measured with an Agilent 4155C semiconductor parameter analyzer. Photocurrent action spectra were obtained using a monochromator (Cornerstone 130 1/8 m) equipped with commercially available gratings and filters (Newport Corp.) in conjunction with a Keithley 2400 source meter controlled by customized LabView code.

## Results and Discussion

**1. Optical and Thermal Properties of P3HTV.** We determined the extinction coefficient ( $\epsilon \sim 4.08 \times 10^4 \text{ cm}^{-1}$  at  $\lambda_{\text{max}} = 574 \text{ nm}$ ) of spin-coated P3HTV films from a plot of absorption versus P3HTV film thickness (see Figure S1 in the Supporting Information). This extinction is approximately 50% of the value of P3HT, which is  $\epsilon \sim 7.86 \times 10^4 \text{ cm}^{-1}$  at 520 nm. Thus, to absorb 99% of light at 574 nm, a  $\sim 245 \text{ nm}$  thick P3HTV film is needed. This estimation does not account for the reflection of the Al contact (i.e., double-pass effect). Figure 2a shows the DSC thermogram of P3HTV at a scan rate of  $10\text{ }^\circ\text{C}/\text{min}$ . P3HTV is a semicrystalline polymer showing melting temperatures ( $T_m$ ) at  $179\text{ }^\circ\text{C}$  ( $2.11\text{ J/g}$ ) in the first heating; the small peaks at  $207$  and  $202\text{ }^\circ\text{C}$  may originate from different crystallite forms. However, in the second heating curve, we have observed a very weak broad peak at  $T_m = 173\text{ }^\circ\text{C}$  ( $0.76\text{ J/g}$ ), indicating a very low level of crystallinity. We observed the glass transition temperature ( $T_g$ ) at  $52\text{ }^\circ\text{C}$ , which is higher than  $T_g \approx -14\text{ }^\circ\text{C}$  of regioregular P3HT<sup>54</sup> and leads to structural stability of films at room temperature. In addition, a TGA thermogram is shown in Figure 2b. P3HTV was stable at least up to  $300\text{ }^\circ\text{C}$  under  $\text{N}_2$ , whereas  $\sim 20\%$  of the material was lost at  $400\text{ }^\circ\text{C}$ .

**2. Structure and Morphology of P3HTV/PCBM Films.** WAXS was carried out on drop-cast films of P3HTV/PCBM blends to investigate not only crystal structure but also phase behavior, including the PCBM solubility limit. Figure 3 shows the WAXS pattern for the P3HTV/PCBM film as a function of PCBM wt %. Out-of-plane WAXS and in-plane grazing-incidence X-ray scattering (GIXS) patterns for the as-deposited films are shown in Figure 3a,b. For pure P3HTV, the magnified WAXS data along with a proposed unit cell for P3HTV are displayed in Figure S2 in the Supporting Information. WAXS peaks are observed at  $q_z = 0.56 \text{ \AA}^{-1}$  ( $2\theta = 7.8$ ,  $d$  spacing = 1.1 nm) and  $1.10 \text{ \AA}^{-1}$  ( $2\theta = 15.5$ ,  $d$  spacing = 0.57 nm); see Figures 3a and S2 in the Supporting Information. By analogy to P3HT WAXS data, we tentatively assign the  $q_z = 0.56 \text{ \AA}^{-1}$  peak to scattering from lamellae arising from interdigitated side-chain packing of the P3HTV molecules. According to our

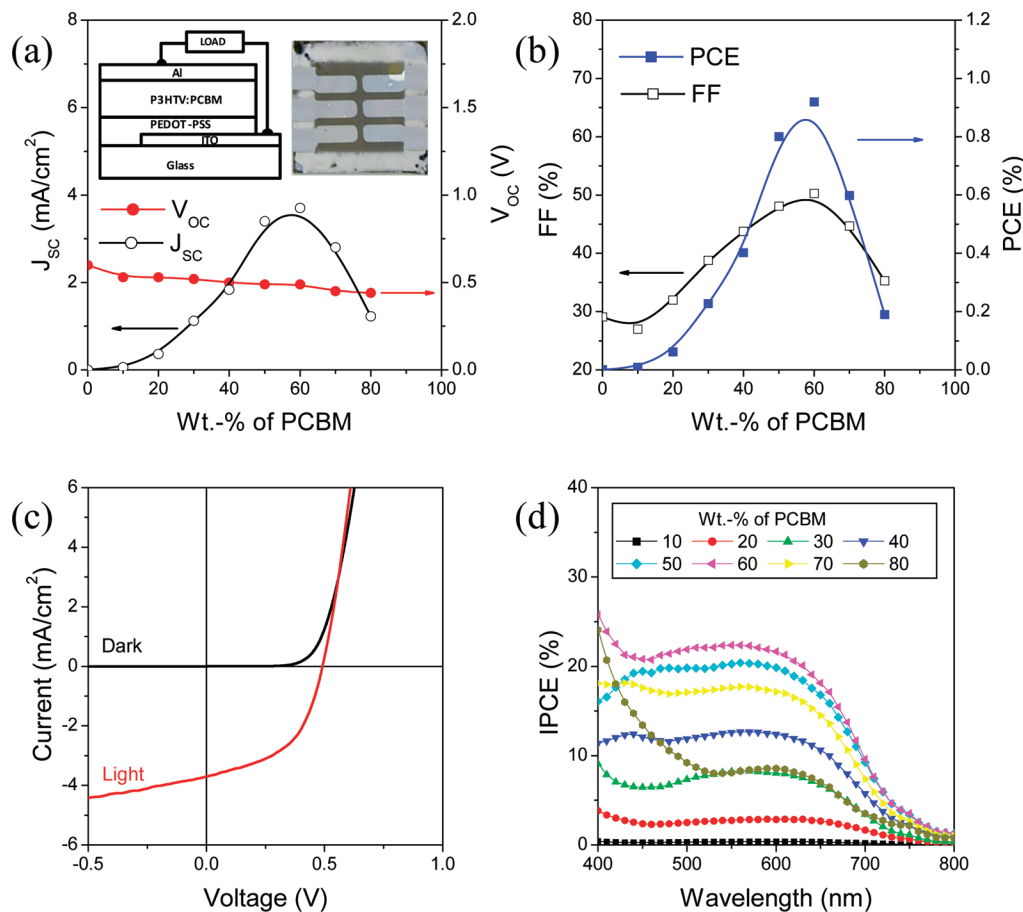


**Figure 6.** Composition dependence of the P3HTV/PCBM solar cells: (a)  $J_{sc}$  and  $V_{oc}$ , under simulated AM 1.5 spectrum, inset shows device structure and picture of P3HTV/PCBM = 40:60 solar cell; (b) FF and PCE under simulated AM 1.5 spectrum; (c)  $J$ – $V$  characteristics of the ~200 nm thick P3HTV/PCBM = 40:60 solar cells under simulated AM 1.5 spectrum and in the dark; and (d) photocurrent action spectra of PV devices under illumination with monochromatic light.

proposed unit cell, this peak would be indexed as (100) and the peak at  $1.10 \text{ \AA}^{-1}$  would be from (200). The P3HTV crystallite size in the [100] direction was estimated from Scherrer's equation ( $t = 0.9 \lambda/B \cos \theta$ ) to be 19.4 nm ( $B = 0.00716 \text{ rad}$ ,  $\theta = 3.93^\circ$ ; untreated film), where  $B$  is the full width at half-maximum (fwhm) of the peak at angle  $\theta$  and  $\lambda$  is the X-ray wavelength.<sup>54,55</sup> Therefore, the crystal size of P3HTV (~19.4 nm) is slightly larger than that of typical P3HT (~13.7 nm),<sup>54</sup> and the (100)  $d$  spacing of P3HTV (~1.1 nm) is smaller than that of P3HT (~1.6 nm), meaning more compact packing of P3HTV molecules in the [100] direction.<sup>54</sup> The WAXS (010) peak corresponding to the  $\pi$ – $\pi$  stacking distance is also very weakly displayed at  $q_x = 1.33 \text{ \AA}^{-1}$  ( $2\theta = 18.9^\circ$ ,  $d$  spacing = 0.47 nm) in Figure S2 in the Supporting Information. For P3HTV/PCBM films in Figure 3a,b, the broad bump at  $q_z = 1.39 \text{ \AA}^{-1}$  ( $d$  spacing = 0.45 nm) is usually observed, which is just the amorphous halo of these blend films, that is, not related with the phase-separated PCBM.

As in our previous study,<sup>54</sup> to observe the PCBM solubility limit clearly, we annealed the P3HTV/PCBM films extensively at 150 °C (lower than  $T_m$  of P3HTV) for 24 h under an argon environment and repeated the WAXS studies in Figure 3c,d. After the annealing step, P3HTV (100) crystallites were observed up to 80 wt % PCBM in Figure 3c. At 0–30 wt % PCBM, GIXS (100) peaks were weak or nonexistent. This observation suggests that, after they are annealed, the P3HTV main chains are more parallel to the silicon substrate or the side chains are more perpendicular to it than in the as-deposited condition. Importantly, we detected sharp PCBM peaks at 50%

PCBM. This result did not change after additional annealing at 150 °C for 72 h, which suggests that equilibrium has been obtained over this time scale. Thus, above 50% PCBM, the blend is phase-separated to form pure PCBM domains coexisting with saturated P3HTV domains at room temperature. On the basis of this analysis, we conclude that the solubility limit of PCBM in P3HTV is 30–50%.

We also studied the surface morphology and, more specifically, the phase lag of the P3HTV/PCBM blend films with various compositions using an AFM operating in tapping mode. The film samples were prepared in the same manner as that for the PV devices. Figure 4 represents the height (left column) and corresponding phase lag (right column) images of P3HTV/PCBM blend films of different compositions.

In the case of pure P3HTV film, that is, 0% PCBM, the phase image shows fiberlike structures with a width of 20–40 nm. This phase contrast in a pure film reflects the semicrystalline nature of P3HTV films, that is, pure P3HTV films having both crystalline and amorphous regions. A critical change takes place in the phase image on increasing the PCBM composition from 40 to 50% in the blend. Whereas both the compositions show considerable phase contrast, the 50% phase image also demonstrates evenly distributed circular domains in a  $1 \times 1 \mu\text{m}^2$  that is not visible in the 40% phase image. We believe that this peculiar contrast in the phase image arises from phase separation at ~50% composition, which supports our WAXS data. The separate phases appear to be granular in nature, as opposed to fibrous, indicating a substantial change in the microstructure of P3HTV/PCBM blends with changing PCBM content. Similar

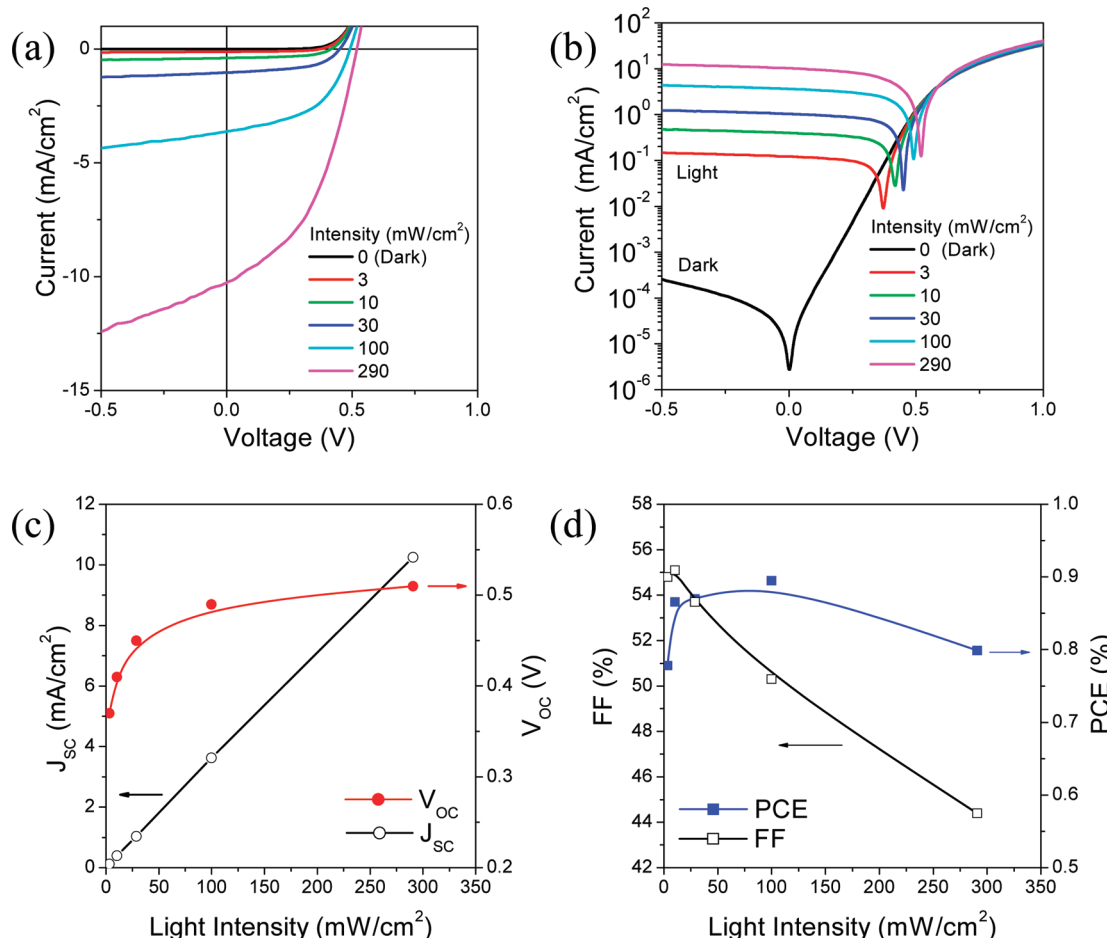


**Figure 7.** Light intensity dependence of the  $\sim 200$  nm thick P3HTV/PCBM = 40:60 solar cells: (a)  $J$ – $V$  characteristics under white light with various intensities, (b) semilog  $J$ – $V$  curve under white light with various intensities, (c)  $J_{sc}$  and  $V_{oc}$ , and (d) FF and PCE.

phase contrast is also seen at 60%. Fourier transform analysis of the phase images shows no peak for 0, 40, and 80%, but a distinct peak was observed in the case of 50 and 60%. The peak position is an indication of the domain size, which is  $\sim 15$  nm for 50% or  $\sim 20$  nm for 60%. We also performed TEM analysis of all the samples at 80 kV under bright field and obtained similar results (see Figure S3 in the Supporting Information).

Another critical parameter that we extracted from the AFM measurements is the root mean square (rms) roughness of the height images for different compositions of blends. Interestingly, rms roughness decreases with an increase in PCBM wt % in the blend: 4–3.5 nm (0–40%), 1.2 nm (50%), and 0.5 nm (60–80%). This behavior can possibly be explained by the following: (1) a pure P3HTV film has large fibrous semicrystals, which may increase surface roughness, (2) the PCBM small molecule shows smooth film-forming properties, and (3) higher content of PCBM destroys the semicrystalline nature of P3HTV (see WAXS data in Figure 3). At this point, it is noteworthy that this trend is exactly opposite to that observed in blends of PCBM with the amorphous polymer, poly(2-methoxy-5-(3',7'-dimethyloctyloxy)-*p*-phenylene vinylene) (MDMO-PPV).<sup>56</sup> Perhaps this is because destruction of crystallinity does not apply to MDMO-PPV.

**3. Transport Behavior in a Transistor Testbed.** With this information, we have examined electrical transport in P3HTV/PCBM transistors to determine the relationship between phase behavior and charge mobility (Figure 5). The field effect hole mobility of the pure P3HTV film is  $2 \times 10^{-4} \text{ cm}^2/(\text{V s})$ , as shown in Figure S4 in the Supporting Information. For unan-

nealed films, the hole mobilities are approximately constant between 0 and 70% PCBM ( $2-5 \times 10^{-4} \text{ cm}^2/(\text{V s})$ ), followed by a gradual decrease. Recall that, from Figure 3a, the absence of P3HTV crystallite WAXS peaks at 80% PCBM or greater indicates that 70–80% is the transition point between semicrystalline and amorphous polymer. PCBM suppresses crystallinity in P3HTV, and this is consistent with lowering of the hole mobility for PCBM concentrations  $>70\%$ .

In contrast, for the as-cast (unannealed) films, no electron mobility was observed until the PCBM concentration exceeded 50%. This composition concurs with the PCBM solubility limit determined by WAXS, AFM, and TEM. Thus, as shown in our previous study,<sup>54</sup> ambipolar (electron and hole) transport was observed only after phase separation, in which a percolating pathway for n-channel conduction seems to be well-formed. Furthermore, after the film was annealed, the electron mobility increased in the intermediate composition range (50–80%). Figure S5 in the Supporting Information shows comparable electron ( $\mu_e = 7 \times 10^{-4} \text{ cm}^2/(\text{V s})$ ) and hole ( $\mu_h = 5 \times 10^{-4} \text{ cm}^2/(\text{V s})$ ) mobilities at a P3HTV/PCBM = 50:50 blend film. However, after the film was annealed, the hole mobilities decreased, presumably from unfavorable morphologies despite the size increase of P3HTV crystallites.

**4. Solar Cell Composition Dependence.** PV devices were fabricated with the ITO/PEDOT/PSS (30 nm)/P3HTV/PCBM ( $\sim 200$  nm)/Al configuration; see Figure 6a, inset (left, device structure; right, picture of a P3HTV/PCBM = 40:60 solar cell). Figure 6a,b shows the P3HTV/PCBM solar cell performance as a function of increasing PCBM composition under 100 mW/

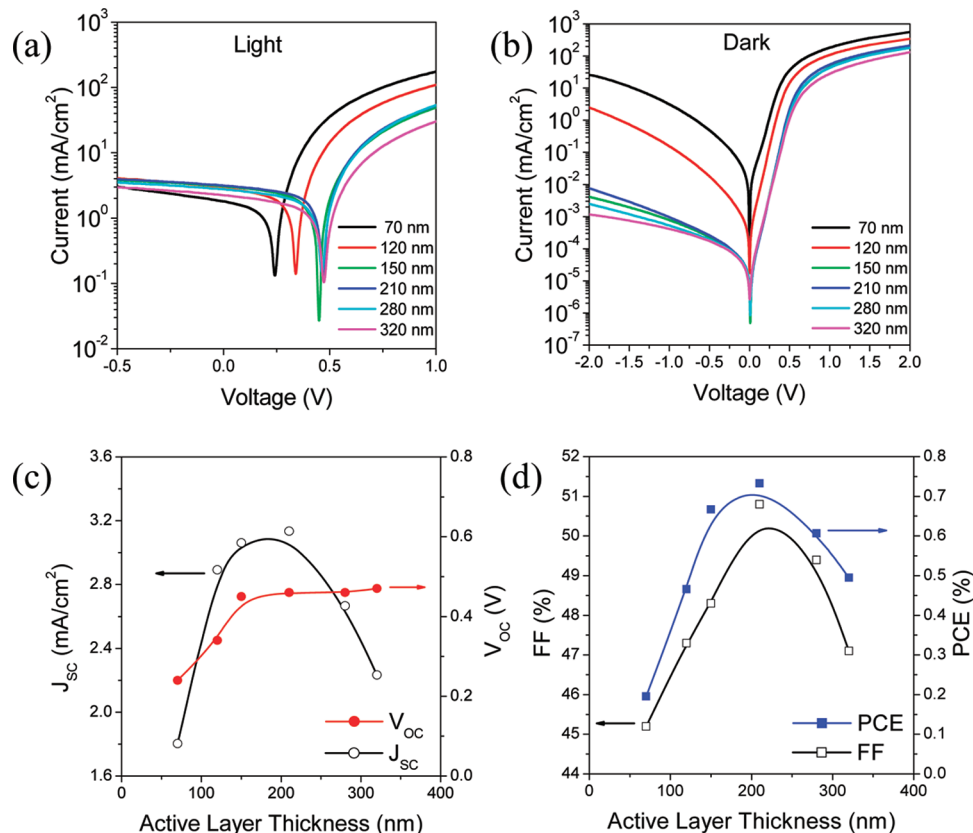


**Figure 8.** Active layer thickness dependence of the P3HTV/PCBM = 40:60 solar cells: (a)  $J$ – $V$  characteristics under simulated AM 1.5 spectrum, (b)  $J$ – $V$  characteristics in the dark, (c)  $J_{sc}$  and  $V_{oc}$  under simulated AM 1.5 spectrum, and (d) FF and PCE under simulated AM 1.5 spectrum.

**TABLE 1: Shunt Resistance, Series Resistance, and Rectification Ratio of P3HTV/PCBM = 40:60 Solar Cells as a Function of Photoactive Layer Thickness**

	70 nm	120 nm	150 nm	210 nm	280 nm	320 nm
$R_p A$ ( $\Omega \cdot \text{cm}^2$ ) (at $V=0$ V)	$2.5 \times 10^3$	$6.8 \times 10^4$	$1.5 \times 10^6$	$1.9 \times 10^6$	$1.7 \times 10^6$	$1.7 \times 10^6$
$R_s A$ ( $\Omega \cdot \text{cm}^2$ ) (at $V=2$ V)	$2.7 \times 10^0$	$4.3 \times 10^0$	$5.8 \times 10^0$	$5.9 \times 10^0$	$6.7 \times 10^0$	$8.0 \times 10^0$
RR [at $V=\pm 2$ V]	$2.1 \times 10^1$	$1.4 \times 10^2$	$5.1 \times 10^4$	$2.8 \times 10^4$	$7.2 \times 10^4$	$1.1 \times 10^5$

$\text{cm}^2$  simulated AM 1.5 irradiation.  $J_{sc}$ , FF, and PCE all show a maximum at  $\sim 50\text{--}60\%$  PCBM.  $V_{oc}$ , on the other hand, gradually decreased from 0.60 V (pure P3HTV) to 0.44 V (80%) with increasing PCBM compositions. If we consider the estimated HOMO ( $= -5.0$  eV) of P3HTV and the LUMO ( $= -4.3$  eV) of PCBM, the measured  $V_{oc}$  is less than the expected maximum value of 0.7 V.<sup>16,56</sup> It has been reported that  $V_{oc}$  is dependent on the BHJ film morphology.<sup>57</sup> Thus, a morphology change with increasing PCBM composition is likely bringing forth this behavior. Importantly, the best performance of solar cells was observed at the  $\sim 50\text{--}60\%$  PCBM, that is, near the phase separation point at which PCEs were 0.80–0.92%.

Figure 6c shows light (100 mW/cm<sup>2</sup>) and dark current–voltage characteristics for the best performing device measured to date, a 60% PCBM blend. This cell showed  $V_{oc} = 0.49$  V,  $J_{sc} = 3.7$  mA/cm<sup>2</sup>, FF = 50.5%, and PCE = 0.92%.<sup>58</sup> Figure 6d shows photocurrent action spectra of PV devices under illumination with monochromatic light as a function of PCBM composition. The spectra show that the P3HTV/PCBM blends can harvest energy across most of the visible spectrum, that is, wavelengths less than 750 nm. The 50–60% PCBM solar cells display about  $\sim 20.2\text{--}22.3\%$  peak external quantum efficiency or incident photon-to-current efficiency (IPCE). The IPCE graph follows the absorption spectra of P3HTV and PCBM; see Figure S6a in the Supporting Information.

**5. Solar Cell Light Intensity Dependence.** Using a series of neutral density of filters, we have studied the P3HTV/PCBM solar cell performance as a function of increasing light intensity,  $I_L$ , ranging from 3 to 290 mW/cm<sup>2</sup>. The  $J$ – $V$  characteristics and intensity dependence of  $J_{sc}$ ,  $V_{oc}$ , FF, and PCE are shown in Figure 7. For the optimal composition, 60% PCBM, short circuit current is essentially linear with light intensity. Fitting to a power law relationship,<sup>56</sup>  $J_{sc} \sim I_L^\alpha$ , yields  $\alpha = 0.98$ . Indeed, for all compositions past the point of phase separation, 50% or above,  $\alpha$  is consistently 0.97–0.98. Below 50%, however,  $\alpha$  begins to decrease, reaching a minimum of 0.92 for the 10% PCBM blend. Whereas the decrease seen here is only slight, sublinear  $\alpha$  dependence has been observed previously for other donor/PCBM systems.<sup>43,44,56</sup> One explanation for this reduction is an increased importance of charge recombination at higher carrier concentrations.

As expected from the relationship  $V_{oc} = V_t \ln(J_{sc}/J_s + 1)$ , where  $V_t$  is the thermal voltage and  $J_s$  is the ideal reverse-bias saturation current,<sup>62</sup>  $V_{oc}$  increases abruptly at low intensity ( $< 50$  mW/cm<sup>2</sup>) before saturating at higher intensities. FF, on the other hand, decreases nonlinearly with light intensities greater than 10 mW/cm<sup>2</sup>, owing to the enhanced possibility of recombination loss and series resistance. Due to this trade-off between  $V_{oc}$  and FF, the overall PCE shows a maximum near 100 mW/cm<sup>2</sup>.

**6. Solar Cell Thickness Dependence.** We have also examined the P3HTV/PCBM (=40:60) solar cell performance as a

function of increasing photoactive layer thickness, seen in Figure 8a,b. Thickness is an important design parameter in solar cell architectures because it determines the optimum balance between light absorption and charge extraction. Table 1 gives the dark currents in terms of series resistance ( $R_s A$ ), shunt resistance ( $R_p A$ ), and rectification ratio (RR).  $R_s A$  and  $R_p A$  were determined from the slope of the dark current–voltage curve at 2 and 0 V, respectively. RR was calculated from the ratio of absolute current values at  $\pm 2$  V. The solar cell parameters are summarized in Figure 8c,d.  $J_{sc}$  increases with thicknesses up to  $\sim 210$  nm and then decreases, owing to increased series resistance and recombination loss.

$V_{oc}$  increases up to  $\sim 150$  nm and levels off at higher thicknesses. The lower  $V_{oc}$  of the thin films (70–120 nm) is attributed to parasitic leakage current caused by film defects, such as pinholes. The 70 and 120 nm thick films show a  $R_p A$  of  $\sim 10^3$  and  $\sim 10^4 \Omega \cdot \text{cm}^2$ , respectively, whereas all thicker films have a  $R_p A \sim 10^6 \Omega \cdot \text{cm}^2$ . FF shows a maximum like the  $J_{sc}$  curves due to recombination loss and series resistance in thicker ( $>210$  nm) films. Thus, the overall device performance is optimized for a  $\sim 210$  nm thick film with a PCE of 0.73%.<sup>58</sup>

## Conclusion

A semicrystalline P3HTV synthesized by ADMET polymerization has been used as an electron donor material in P3HTV/PCBM BHJ solar cells. The photoactive P3HTV blends were studied as a function of increasing PCBM compositions using WAXS, AFM, and TEM. The PCBM solubility limit is  $\sim 50\%$  PCBM. Second, we have studied the relationship between electrical transport and phase behavior. Below the PCBM solubility limit ( $\sim 50$  wt %), only hole transport was observed, and above the solubility limit, ambipolar (electron and hole) transport was shown. Finally, we have fabricated a series of P3HTV/PCBM solar cells, finding an optimum in performance of 0.80–0.92% PCE for  $\sim 200$  nm thick, 50–60 wt % PCBM blends, just about the 50 wt % PCBM phase-separation composition. We believe that optimization of the P3HTV molecular weight and regioregularity may enhance carrier mobilities in this architecture. Further optimization of the device may also bring forth improved power conversion.

**Acknowledgment.** This work was funded by the Initiative for Renewable Energy and the Environment (IREE) at the University of Minnesota (UMN) and the Xcel Energy Renewable Development Fund. It was also supported by the UMN Materials Research Science and Engineering Center (MRSEC), funded by the NSF (DMR-0212302), and also partly funded through DMR-0706011. Parts of this work were carried out at the Institute of Technology Characterization Facility, UMN, which receives partial support from NSF through the NNIN program. C.D.F. thanks Prof. Russell Holmes for making his solar cell testing equipment available.

**Supporting Information Available:** UV-vis absorption spectra as a function of PCBM composition or film thickness, WAXS data for P3HTV film, TEM images, and current–voltage characteristics for P3HTV-based transistors are included. This material is available free of charge via the Internet at <http://pubs.acs.org>.

## References and Notes

- (1) Halls, J. J. M.; Walsh, C. A.; Greenham, N. C.; Marseglia, E. A.; Friend, R. H.; Moratti, S. C.; Holmes, A. B. *Nature* **1995**, *376*, 498–500.
- (2) Yu, G.; Gao, J.; Hummelen, J. C.; Wudl, F.; Heeger, A. J. *Science* **1995**, *270*, 1789–1791.
- (3) Gregg, B. A. *J. Phys. Chem. B* **2003**, *107*, 4688–4698.
- (4) Coakley, K. M.; McGehee, M. D. *Chem. Mater.* **2004**, *16*, 4533–4542.
- (5) Li, G.; Shrotriya, V.; Huang, J.; Yao, Y.; Moriarty, T.; Emery, K.; Yang, Y. *Nat. Mater.* **2005**, *4*, 864–868.
- (6) Ma, W.; Yang, C.; Gong, Y.; Lee, K.; Heeger, A. J. *Adv. Funct. Mater.* **2005**, *15*, 1617–1622.
- (7) Reyes-Reyes, M.; Kim, K.; Carroll, D. L. *Appl. Phys. Lett.* **2005**, *87*, 083506/1–083506/3.
- (8) Kim, Y.; Cook, S.; Tuladhar, S. M.; Choulis, S. A.; Nelson, J.; Durrant, J. R.; Bradley, D. D. C.; Giles, M.; Mcculloch, I.; Ha, C.-S.; Ree, M. *Nat. Mater.* **2006**, *5*, 197–203.
- (9) Wong, W.-Y.; Wang, X.-Z.; He, Z.; Djurišić, A. B.; Yip, C.-T.; Cheung, K.-Y.; Wang, H.; Mak, C. S. K.; Chan, W.-K. *Nat. Mater.* **2007**, *6*, 521–527.
- (10) Gunes, S.; Neugebauer, H.; Sariciftci, N. S. *Chem. Rev.* **2007**, *107*, 1324–1338.
- (11) Blom, P. W. M.; Mihailescu, V. D.; Koster, L. J. A.; Markov, D. E. *Adv. Mater.* **2007**, *19*, 1551–1566.
- (12) Yang, X.; Loos, J. *Macromolecules* **2007**, *40*, 1353–1362.
- (13) Mayer, A. C.; Scully, S. R.; Hardin, B. E.; Rowell, M. W.; McGehee, M. D. *Mater. Today* **2007**, *10*, 28–33.
- (14) Thompson, B. C.; Fréchet, M. J. *Angew. Chem., Int. Ed.* **2008**, *47*, 58–77.
- (15) Koster, L. J. A.; Mihailescu, V. D.; Blom, P. W. M. *Appl. Phys. Lett.* **2006**, *88*, 093511/1–093511/3.
- (16) Scharber, M. C.; Mühlbacher, D.; Koppe, M.; Denk, P.; Waldauf, C.; Heeger, A. J.; Brabec, C. J. *Adv. Mater.* **2006**, *18*, 789–794.
- (17) Roncali, J. *Chem. Rev.* **1997**, *97*, 173–205.
- (18) Van Duren, J. K. J.; Dhanabalan, A.; van Hal, P. A.; Janssen, R. A. J. *Synth. Met.* **2001**, *121*, 1587–1588.
- (19) Svensson, M.; Zhang, F.; Veenstra, S. C.; Verhees, W. J. H.; Hummelen, J. C.; Kroon, J. M.; Inganäs, O.; Andersson, M. R. *Adv. Mater.* **2003**, *15*, 988–991.
- (20) Winder, C.; Sariciftci, N. S. *J. Mater. Chem.* **2004**, *14*, 1077–1086.
- (21) Mühlbacher, D.; Scharber, M.; Morana, M.; Zhu, Z.; Waller, D.; Gaudiana, R.; Brabec, C. *Adv. Mater.* **2006**, *18*, 2884–2889.
- (22) Bundgaard, E.; Krebs, F. C. *Sol. Energy Mater. Sol. Cells* **2007**, *91*, 954–985.
- (23) Peet, J.; Kim, J. Y.; Coates, N. E.; Ma, W. L.; Moses, D.; Heeger, A. J.; Bazan, G. C. *Nat. Mater.* **2007**, *6*, 497–500.
- (24) Li, Y.; Zou, Y. *Adv. Mater.* **2008**, *20*, 2952–2958.
- (25) <http://frede.nrel.gov/solar/spectra/am1.5>.
- (26) Zhan, X.; Tan, Z.; Domercq, B.; An, Z.; Zhang, X.; Barlow, S.; Li, Y.; Zhu, D.; Kippelen, B.; Marder, S. R. *J. Am. Chem. Soc.* **2007**, *129*, 7246–7247.
- (27) Wienk, M. M.; Turbiez, M.; G, R.; Struijk, M. P.; Fonrodona, M.; Janssen, R. A. J. *Appl. Phys. Lett.* **2006**, *88*, 153511/1–153511/3.
- (28) Blouin, N.; Michaud, A.; Leclerc, M. *Adv. Mater.* **2007**, *19*, 2295–2300.
- (29) Wang, E.; Wang, L.; Lan, L.; Luo, C.; Zhuang, W.; Peng, J.; Cao, Y. *Appl. Phys. Lett.* **2008**, *92*, 033307/1–033307/3.
- (30) Huitema, H. E. A.; Gelink, G. H.; van der Putten, J. B. P. H.; Kuijk, K. E.; Hart, C. M.; Cantatore, E.; Herwig, P. T.; van Breemen, A. J. J. M.; de Leeuw, D. M. *Nature* **2001**, *414*, 599.
- (31) Fuchigami, H.; Tsumura, T.; Koezuka, H. *Appl. Phys. Lett.* **1993**, *63*, 1372–1374.
- (32) Yamada, S.; Tokito, S.; Tsutsui, T.; Saito, S. *J. Chem. Soc., Chem. Commun.* **1987**, 1448–1449.
- (33) Henckens, A.; Knipper, M.; Polec, I.; Manca, J.; Lutsen, L.; Vanderzande, D. *Thin Solid Films* **2004**, *451*–452, 572–579.
- (34) Smith, A. P.; Smith, R. R.; Taylor, B. E.; Durstock, M. F. *Chem. Mater.* **2004**, *16*, 4687–4692.
- (35) Hou, J.; Tan, Z.; He, Y.; Yang, C.; Li, Y. *Macromolecules* **2006**, *39*, 4657–4662.
- (36) Nguyen, L. H.; Günes, S.; Neugebauer, H.; Sariciftci, N. S.; Banishoeib, F.; Henckens, A.; Cleij, T. J.; Lutsen, L.; Vanderzande, D. *Sol. Energy Mater. Sol. Cells* **2006**, *90*, 2815–2828.
- (37) Banishoeib, F.; Henckens, A.; Fourier, S.; Vanhooyland, G.; Breselge, M.; Manca, J.; Cleij, T. J.; Lutsen, L.; Vanderzande, D.; Nguyen, L. H.; Neugebauer, H.; Sariciftci, N. S. *Thin Solid Films* **2008**, *516*, 3978–3988.
- (38) Girotto, C.; Cheyns, D.; Aernouts, T.; Banishoeib, F.; Lutsen, L.; Cleij, T. J.; Vanderzande, D.; Genoe, J.; Poortmans, J.; Heremans, P. *Org. Electron.* **2008**, *9*, 740–746.
- (39) Qin, Y.; Hillmyer, M. A. Manuscript submitted to *Macromolecules*, 2009.
- (40) Lehman, S. E., Jr.; Wagener, K. B. In *Handbook of Metathesis*; Grubbs, R. H., Ed.; Wiley-VCH Verlag GmbH & Co.: KGaA, Weinheim, Germany, 2003; Vol. 3.
- (41) Kim, Y.; Choulis, S. A.; Nelson, J.; Bradley, D. D. C.; Cook, S.; Durrant, J. R. *J. Mater. Chem.* **2005**, *40*, 1371–1376.

- (42) Mihailetschi, V. D.; Koster, L. J. A.; Blom, P. W. M.; Melzer, C.; de Boer, B.; van Duren, J. K. J.; Janssen, R. A. J. *Adv. Funct. Mater.* **2005**, *15*, 795–801.
- (43) Schilinsky, P.; Waldauf, C.; Brabec, C. *J. Appl. Phys. Lett.* **2002**, *81*, 3885–3887.
- (44) Mihailetschi, V. D.; Blom, P. W. M.; Hummelen, J. C.; Rispens, M. T. *J. Appl. Phys.* **2003**, *94*, 6849–6854.
- (45) Yoo, S.; Domercq, B.; Kippelen, B. *J. Appl. Phys.* **2005**, *97*, 103706/1–103706/9.
- (46) Koster, L. J. A.; Mihailetschi, V. D.; Ramaker, R.; Blom, P. W. M. *Appl. Phys. Lett.* **2005**, *86*, 123509/1–123509/3.
- (47) Koster, L. J. A.; Mihailetschi, V. D.; Xie, H.; Blom, P. W. M. *Appl. Phys. Lett.* **2005**, *87*, 203502/1–203502/3.
- (48) Mihailetschi, V. D.; Xie, H. X.; de Boer, B.; Koster, L. J. A.; Blom, P. W. M. *Adv. Funct. Mater.* **2006**, *16*, 699–708.
- (49) Marsh, R. A.; McNeill, C. R.; Abrusci, A.; Campbell, A. R.; Friend, R. H. *Nano Lett.* **2008**, *8*, 1393–1398.
- (50) Li, G.; Shrotriya, V.; Yao, Y.; Yang, Y. *J. Appl. Phys.* **2005**, *98*, 043704/1–043704/5.
- (51) Moulé, A. J.; Bonekamp, J. B.; Meerholz, K. *J. Appl. Phys.* **2006**, *100*, 094503/1–094503/7.
- (52) Lenes, M.; Koster, L. J. A.; Mihailetschi, V. D.; Blom, P. W. M. *Appl. Phys. Lett.* **2006**, *88*, 243502/1–243502/3.
- (53) Qin, Y.; Kim, J. Y.; Frisbie, C. D.; Hillmyer, M. A. *Macromolecules* **2008**, *41*, 5563–5570.
- (54) Kim, J. Y.; Frisbie, C. D. *J. Phys. Chem. C* **2008**, *112*, 17726–17736.
- (55) Cullity, B. D.; Stock, S. R. *Elements of X-Ray Diffraction*; Prentice Hall: Upper Saddle River, NJ, 2001.
- (56) Van Duren, J. K. J.; Yang, X.; Loos, J.; Bulle-Lieuwma, C. W. T.; Sieval, A. B.; Hummelen, J. C.; Janssen, R. A. J. *Adv. Funct. Mater.* **2004**, *14*, 425–434.
- (57) Liu, J.; Shi, Y.; Yang, Y. *Adv. Funct. Mater.* **2001**, *11*, 420–424.
- (58) Devices show some degree of variation from batch to batch of P3HTV polymer. After testing several tens of solar cells, a second batch of P3HTV polymer consistently gave slightly lower  $J_{sc}$  (average = 3.2 mA/cm<sup>2</sup>), resulting in efficiencies of near 0.7%. Variation of regioregularity and molecular weight distribution could significantly impact device performance.<sup>59,60</sup> A detailed study of the optimization of P3HTV synthesis and its correlation with device performance will be included in future work. In addition, our manuscript of P3HTV-based bilayer solar cells was submitted.<sup>61</sup>
- (59) Sivula, K.; Luscombe, C. K.; Thomson, B. C.; Fréchet, J. M. J. *J. Am. Chem. Soc.* **2006**, *128*, 13988–13989.
- (60) Woo, C. H.; Thomson, B. C.; Kim, B. J.; Toney, M. F.; Fréchet, J. M. J. *J. Am. Chem. Soc.* **2008**, *130*, 16324–16329.
- (61) Stevens, D. M.; Qin, Y.; Hillmyer, M. A.; Frisbie, C. D. *J. Phys. Chem. C* **2009**, in press.
- (62) Sze, S. M. *Physics of Semiconductor Devices*; John Wiley & Sons, Inc.: New York, 1981.

JP902199Q